arXiv:1107.0544v6 [cond-mat.mtrl-sci] 8 Mar 2012

MEAM potentials for Al, Si, Mg, Cu, and Fe alloys

B. Jelinek, S. Groh,* and M. F. Horstemeyer†
Center for Advanced Vehicular Systems, 200 Research Boulevard, Starkville, MS 39759

J. Houze and S. G. Kim‡
Department of Physics and Astronomy, Mississippi State University, Mississippi State, MS 39762

G. J. Wagner
Sandia National Laboratories, P.O. Box 969, MS 9401, Livermore, CA 94551

A. Moitra
Department of Chemical Engineering, The Pennsylvania State University, University Park, PA 16802

M. I. Baskes§
Mechanical and Aerospace Engineering, University of California in San Diego, La Jolla, CA 92093
(Dated: March 12, 2012)

A set of Modified Embedded Atom Method (MEAM) potentials for the interactions between Al, Si, Mg, Cu, and Fe was developed from a combination of each element's MEAM potential in order to study metal alloying. Previously published MEAM parameters of single elements have been improved for better agreement to the generalized stacking fault energy (GSFE) curves when compared with ab-initio generated GSFE curves. The MEAM parameters for element pairs were constructed based on the structural and elastic properties of element pairs in the NaCl reference structure garnered from ab-initio calculations, with adjustment to reproduce the ab-initio heat of formation of the most stable binary compounds. The new MEAM potentials were validated by comparing the formation energies of defects, equilibrium volumes, elastic moduli, and heat of formation for several binary compounds with ab-initio simulations and experiments. Single elements in their ground state crystal structure were subjected to heating to test the potentials at elevated temperatures. An Al potential was modified to avoid formation of an unphysical solid structure at high temperatures. The thermal expansion coefficient of a compound with the composition of AA 6061 alloy was evaluated and compared with experimental values. MEAM potential tests performed in this work, utilizing the universal Atomistic Simulation Environment (ASE), are distributed to facilitate reproducibility of the results.

PACS numbers: 61.50.Lt, 62.20.D- 61.72.J- 68.35.-p

I. INTRODUCTION

Historically, materials have been developed through the correlation of processing and properties. Several implementations of materials science principles have given birth to an engineering framework for materials design. Over the past two decades, more efficient computational methodologies have been developed and the computational power have increased enormously, making the computational materials design an essential cost-effective tool to design materials properties. Since materials complexities can limit the degree of predictability, several time- and length-scale methodologies (hence spatiotemporal hierarchy) for computational materials design naturally evolved (cf. Horstemeyer [1] for a review). Out of several computational methodologies, atomistic simulations not only can predict the materials properties from a statistical viewpoint, but can also quantify the mechanisms of the structure-property relationship. One of the most critical components of atomistic simulations is the interatomic potential, which determines the forces on individual atoms. First-principles calculations certainly are capable of providing very reliable interatomic potentials in a variety of chemical environments. However, realistic simulations of alloy systems, which are essential to reveal many macroscopic materials properties, often require a number of atoms that renders these methods impractical – they either require too much computer memory or take too long to be completed in a reasonable amount of time. One alternative is to use (semi-)empirical interaction potentials that can be evaluated efficiently, so that the atomistic approaches that use them can, in certain cases, handle systems with more than a million atoms.

The Embedded-Atom Method (EAM) is a widely used atomic level semiempirical model for metals, covalent materials, and impurities[2]. MEAM (Modified EAM) incorporates angular dependency of electron density into EAM. Atomistic simulations of a wide range of elements and alloys have been performed using MEAM potentials. MEAM model was first used for silicon, germanium, and their alloys[3]. It was applied to 26 single elements[4] and to silicon-nickel[5] alloys and interfaces. Gall *et al.*[6] have used MEAM to model tensile debonding of an aluminum-silicon interface. Lee and Baskes[7] improved MEAM to account for the second nearest-neighbor interactions. Also, Huang *et al.*[8] used MEAM and two other potentials to deter-

mine defect energetics in beta-SiC. MEAM parameters for nickel[9] and molybdenum-silicon system[10] were determined by Baskes. MEAM potentials for Cu, Ag, Au, Ni, Pd, Pt, Al, and Pb based on the first and the second nearest-neighbor MEAM were constructed by Lee *et al.*[11]. Hu *et al.*[12,13] proposed a new analytic modified EAM many-body potential and applied it to 17 hcp metals. The structural properties of various polytypes of carbon were described using a MEAM potential by Lee and Lee[14]. Recent work of Lee *et al.*[15] summarized available MEAM potentials for single elements and alloys. Several of these potentials were then used to perform large scale atomistic simulations to understand the intriguing nature of the ductile and brittle fracture[16], structure-property relationship[17], dislocation dynamics[18,19], and nature of materials fracture[20,21].

Aluminum, magnesium, copper, and iron alloys are being used in developing materials with novel properties. Great popularity of these alloys is connected to their general functional properties, mechanical properties, mass density, corrosion resistance, and machinability. Light metal alloys, such as magnesium and aluminum alloys, are now demanded for use in the automotive and aviation industries. They performed remarkably well for the purpose of decreasing the operating expenses and fuel consumption. These alloys usually contain several other minor elements, such as silicon, nickel, and manganese, and are known to have very complex phase compositions. Assessment of such complex systems is a very challenging task, since different constituent elements can form different phases, whose selection depends on the ratio between the constituents and also on a variety of processing and treatment factors.

Contrary to DFT potentials, most of the single element semiempirical potentials do not combine easily into multi-component alloy models. The difficulty of combining single element EAM potentials into alloy systems comes from the need of their normalization[22]. The procedure to form EAM alloy parameterization from single element potentials was suggested[23,24], but it does not guarantee that the resulting potential will be suitable for modeling compounds[25]. Alloy potentials usually introduce new parameters for each pair of elements, allowing to fit properties of their binary compounds. The number of parameters to adjust and the number of tests to perform is proportional to the square of the number of constituent elements. In the present MEAM approach, each pair interaction is characterized by a total of 13 parameters (Table V, and the ratio of density scaling factors ρ_0 for constituent elements, Table I). Adoption of the default value $C_{\max} = 2.8$ leads to 9 adjustable parameters for each pair. Comparable angularly dependent potentials for the Fe-Ni system[26] also have 9 adjustable pair parameters.

While the semiempirical potentials have been developed and tested for binary alloys[27–31], binaries, similarly to single element potentials, may not combine easily into ternaries. Modeling of ternary systems faces a challenge since less experimental properties are available for ternary systems. Ternary potentials are usually examined only at a particular composition range—the number of possible compositions grows to the power of the number of constituent elements. It is also nontrivial to find an equilibrium structure for complex systems of representative size at low temperatures. Ternary potentials are only available for Fe/Ni-Cr-O[32] (MEAM), Pu-Ga-He[33] (MEAM), Fe-Ti-C/N, Cu-Zr-Ag, Ga-In-N, Fe-Nb-C/N[34–37] (MEAM), H-C-O[38] (Reactive Force Field, ReaxFF), Ni-Al-H[39], Zr-Cu-Al[40], and Fe-Cu-Ni[41] (EAM) systems. To extend from binaries to ternaries, MEAM provides a ternary screening parameter C^{XYZ}. In the present work we did not examine ternary systems. Instead, we performed thermal expansion simulations of a compound including all species of the potential. The default values of $C_{\min} = 2.0$ and $C_{\max} = 2.8$ were applied for ternary screening. Since an effort beyond the scope of our project is required for satisfiable validation of the 5-element alloy potential under varying temperatures, compositions, and configuration states, we concentrated on basic tests and on providing tools to facilitate reproducibility of the tests[42].

In the present study we develop a MEAM potential for aluminum, silicon, magnesium, copper, iron, and their combinations. We fit the potential to the properties of single elements and element pairs, but the model implicitly allows calculations with any combination of elements. We show the applied MEAM methodology in Appendix A. The DFT calculations are described in Sec. II. In Sec. III, the single-element volume-energy curves in basic crystal structures, and also important material properties, such as formation energies of vacancies, self-interstitials, surfaces, and generalized stacking fault energies from MEAM are examined and compared with DFT calculations. In Sec. IV, the MEAM potential parameters for each unlike element pair are initialized to fit the ab-initio heat of formation, equilibrium volume, and elastic moduli of the hypothetical NaCl reference structure. Heat of formation of binary compounds in a variety of crystal structures from MEAM are thereafter examined and compared with the ab-initio and experimental results. The MEAM parameters are adjusted to match the DFT formation energy of the most stable compounds. The structural and elastic properties for several binary compounds and formation energies of substitutional defects are compared with ab-initio and experimental results. Finally we performed thermal expansion simulations of a compound with the composition of an AA 6061 alloy (IV C). We conclude with a short summary.

II. AB-INITIO CALCULATIONS

Ab-initio total energy calculations in this work were based on density functional theory (DFT), using the projector augmented-wave (PAW) method[43] as implemented in the VASP code[44]. Exchange-correlation effects were treated by the generalized gradient approximation (GGA) as parameterized by Perdew *et al.*[45]. All DFT calcula-

TABLE I. Set of the MEAM potential parameters for single elements. The reference structures for Al, Si, Mg, Cu, and Fe are fcc, diamond, hcp, fcc, and bcc, respectively. E_c is the cohesive energy, a_0 is the equilibrium lattice parameter, A is the scaling factor for the embedding energy, α is the exponential decay factor for the universal energy, $\beta^{(0-3)}$ are the exponential decay factors for the atomic densities, $t^{(0-3)}$ are the weighting factors for the atomic densities, $C_{\max}$ and $C_{\min}$ are screening parameters, ρ_0 is the density scaling factor that is relevant only for element pairs. Definition of these parameters may be found in Ref. 4. Non-zero parameters δ_r in Rose Eq. (B1–B4) were used for Al ($\delta_r = 0.1$) and Fe ($\delta_r = 0.3$), along with $\delta_a = 0.0$.

elem.	E_c[eV]	a_0[Å]	A	α	$\beta^{(0)}$	$\beta^{(1)}$	$\beta^{(2)}$	$\beta^{(3)}$	$t^{(0)}$	$t^{(1)}$	$t^{(2)}$	$t^{(3)}$	$C_{\min}$	$C_{\max}$	ρ_0
Al	3.353	4.05	1.07	4.64	2.04	3.0	6.0	1.5	1.0	4.50	-2.30	8.01	0.8	2.8	1.0
Si	4.63	5.431	1.00	4.87	4.4	5.5	5.5	5.5	1.0	2.05	4.47	-1.80	2.0	2.8	2.2
Mg	1.51	3.194	0.8	5.52	4.0	3.0	0.2	1.2	1.0	10.04	9.49	-4.3	0.8	2.8	0.63
Cu	3.54	3.62	1.07	5.11	3.634	2.2	6.0	2.2	1.0	4.91	2.49	2.95	0.8	2.8	1.1
Fe	4.28	2.851	0.555	5.027	3.5	2.0	1.0	1.0	1.0	-1.6	12.5	-1.4	0.68	1.9	1.0

tions were performed in high precision with the plane-wave cut-off energy set to 400 eV in order to achieve the convergence of heat of formation and elastic properties. Integration over the irreducible Brillouin zone was performed using the Γ-centered Monkhorst-Pack scheme[46] with the size gradually increased to 7×7×7 for point defects, to 19×19×1 for surfaces, and to 29×29×29 to improve convergence of shear moduli at small strains. Elastic constants presented here were obtained without relaxation of atomic positions. Since most of the examined high energy structures are, at best, metastable, relaxation does not maintain the crystal symmetry, resulting in large energy changes and unphysical elastic constants.

III. MEAM PARAMETERS FOR SINGLE ELEMENTS

The present MEAM parameters for single elements are listed in Table I. The initial values of these parameters were taken from existing MEAM potentials[4,11,47,48]. The $C_{\min}$ screening parameter for Al, Mg, and Cu was lowered from 2.0 to 0.8 to improve the GSFE curves (Sec. III E). The Mg potential was adjusted to reproduce the DFT values of hcp, bcc, and fcc energy differences, vacancy formation energy, and $(10\bar{1}0)$ surface formation energy. The Al potential was modified to prevent formation of an unknown structure at elevated temperatures (Sec. IV C).

A. Energy dependence on volume of single elements in fcc, hcp, bcc, and simple cubic crystal structures

The first test of the validity of MEAM potential for single elements is a comparison of the energy-volume curves in the fcc, hcp, bcc, diamond, and simple cubic crystal structures, shown in Fig. 1. The MEAM potentials appropriately capture the lowest energy structures of Al (fcc), Si (dia), Mg (hcp), Cu (fcc), and Fe (bcc). Also, the equilibrium volumes of several crystal structures from MEAM closely match the DFT results. Better match of DFT energy differences and volume ratios can possibly be obtained by optimization of Si and Cu MEAM parameters. Fe MEAM potential applied in the present work is a MEAM-p variant of Fe potential from the recent effort of Lee *et al.*[48], exhibiting a correct low temperature phase stability with respect to the pressure. The fcc equilibrium energy and volume from this Fe potential is very close to the bcc equilibrium in order for the structural transition to appear at finite temperature without magnetic contribution. In general the MEAM potentials of the present work reproduced the DFT results for the individual elements fairly well.

B. Vacancies

The formation energy of a single vacancy E_f^{vac} is defined as the energy cost to create a vacancy:

$$E_f^{vac} = E_{tot}[N] - N\varepsilon, \quad (1)$$

where $E_{tot}[N]$ is the total relaxed energy of a system with N atoms containing a vacancy and ε is the energy per atom in the bulk. Cell volume and atomic positions were relaxed in each case. Table II shows the formation energies of a single vacancy for the fcc Al cell, diamond Si cell, hcp Mg, fcc Cu, and bcc Fe obtained from the MEAM and DFT calculations. The MEAM systems sizes were 5×5×5 primitive fcc and bcc cells, 3×3×3 primitive diamond cells, and 8×4×4 orthogonal hcp cells. For the DFT systems, the simulation sizes were 5×5×5 fcc, 4×4×4 diamond and bcc, and 4×4×2 hcp primitive cells.

The vacancy formation energy of Mg was slightly improved in comparison with previous MEAM results[47]. Overall agreement of vacancy formation energies between MEAM, experiment, and DFT was within a few eV, and the present results are comparable or better than those from other calculations. The reduction in volume due to the formation of a vacancy agrees well with the DFT, except the value for Fe is somewhat low.

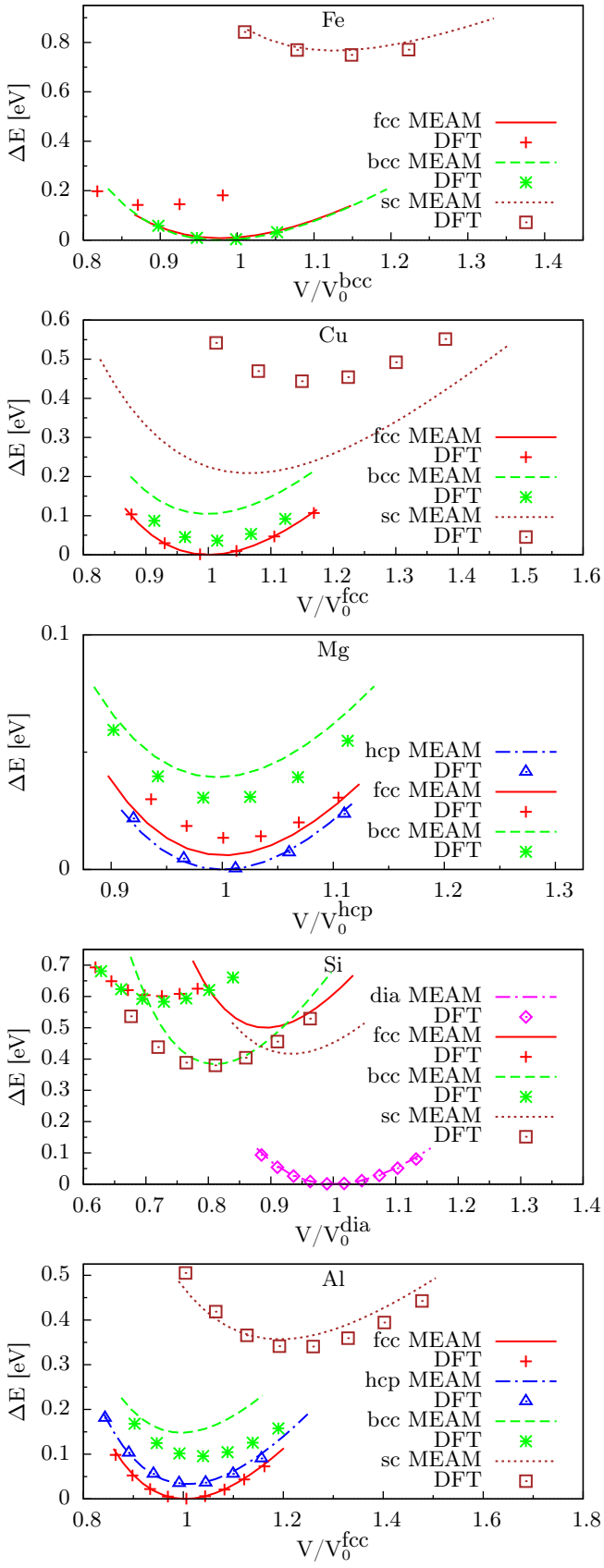

FIG. 1. (Color online) Energy-volume dependence of Al, Si, Mg, Cu, and Fe in fcc, hcp, bcc, diamond, and simple cubic crystal structures relative to the ground state.

TABLE II. Calculated single vacancy properties. Single vacancy formation energy E_f^{vac} and formation volume Ω_v values are obtained from the relaxed structures containing single vacancies. Here Ω_0 is the bulk atomic volume. All energy values are listed in eV. The results from the MEAM calculations are compared with the results from the DFT calculations given inside the parentheses, other simulations, and experiments.

	E_f^{vac}			Ω_v/Ω_0	
	Present	Others	Exp	Present	Others
Al	0.67 (0.5)	0.68[a] 0.68[b] (0.55[f])	0.67[g]	0.67 (0.7)	0.72[a] 0.61[b]
Si	3.27 (3.6)	3.56[t] 3.67[s] (3.6[c])	3.6[i]	0.21 (0.3)	0.94[t]
Mg	0.89 (0.7)	0.59[d] 0.87[b] (0.83[k])	0.79[e]	0.72 (0.8)	0.83[d] 0.87[b]
Cu	1.10 (1.0)	1.05[q] 1.27[r] (1.03[h])	1.2[j]	0.75 (∼0.9)	0.70[r] 0.74[r]
Fe	1.65 (2.1)	1.84[l] 1.89[m] (1.95[n])	1.53[o]	0.47 (∼0.8)	0.6[p] (0.90[n])

[a] MEAM results by Lee *et al.* [11]
[b] Calculated using EAM parameters extracted from Liu *et al.* [49]
[c] DFT calculation by Wright [50]
[d] AMEAM results by Hu *et al.* [12]
[e] Experimental results by Tzanetakis *et al.* [51]
[f] DFT results by Carling *et al.* [52]
[g] Experimental value by Hehenkamp [53]
[h] DFT calculation by Andersson and Simak [54]
[i] Experimental value by Dannefaer *et al.* [55], Throwe *et al.* [55]
[j] Experimental value by Hehenkamp *et al.* [56]
[k] DFT value by Krimmel and Fähnle [57]
[l] EAM value by Mendelev *et al.* [58]
[m] Finnis-Sinclair potential value by Ackland *et al.* [59]
[n] DFT value by Domain and Becquart [60]
[o] Experimental value by Schaefer *et al.* [61]
[p] Experimental value referenced in Ackland *et al.* [59]
[q] EAM value by Mendelev *et al.* [62]
[r] EAM value by Mishin *et al.* [63]
[s] MEAM value by Timonova *et al.* [64]
[t] MEAM value by Ryu *et al.* [65]

C. Self-interstitials

The formation energy of an interstitial point defect E_f^{int} is given by

$$E_f^{int} = E_{tot}[N+1] - N\varepsilon_X - \varepsilon_Y \quad (2)$$

where $E_{tot}[N+1]$ is the total energy of a system with N type-X bulk atoms plus one impurity atom of type-Y inserted at one of the interstitial sites, and ε_X (ε_Y) is the total energy per atom of type-X (type-Y) in its most stable bulk structure. The inserted atom Y can be of the same type as the bulk, in which case the point defect is called a self-interstitial defect. Self-interstitial formation energies were calculated for Al, Si, Mg, and Cu at the octahedral, tetrahedral, and dumbbell sites. Dumbbell orientations were [100] for fcc, [0001] for hcp, and [110] for bcc and diamond structures. Relaxations of the atomic positions and the volume were also performed, and the DFT and MEAM results are listed in Table III. Similar to the previous calculations, the MEAM systems sizes were 5×5×5 primitive fcc and bcc cells, 3×3×3 primitive diamond cells, and 8×4×4 orthogonal hcp cells. For the DFT systems, the examined sizes were 5×5×5 fcc primitive cells, 4×4×4 diamond and bcc primitive cells, and 4×4×2 hcp primitive cells.

TABLE III. The formation energies of various Al, Si, Mg, Cu, and Fe self-interstitials. All energy values are given in eV. The results from the MEAM calculations are compared with the DFT results and other classical MD (CMD) simulations.

Interstitial	DFT	MEAM		CMD		DFT
Al	Present		Ref.[49]	Ref.[66]	Ref.[67]	Ref.[68]
tetrahedral	3.3	3.32	3.16[a]	2.94		
octahedral	2.8	3.26	3.06[a]	2.82		
split (100)	2.7	2.77	2.68[a]	2.46	2.59	2.43
Si	Present		Ref.[69]	Ref.[70]	Ref.[71]	Ref.[72]
split (110)	3.7	3.71	3.88	4.7	3.9	3.40
Mg	Present		Ref.[49]	Ref.[47]	Ref.[73]	Ref.[47]
tetrahedral	2.2	1.63	1.53[a]	1.53	1.41	2.35
octahedral	2.2	1.57	2.16[a]	1.29	1.20	2.36
split (0001)	2.3	1.78	1.52[a]			
Cu	Present		Ref.[62]	Ref.[63]	Ref.[63]	Ref.[62]
tetrahedral	3.9	3.37	2.99[a]			
octahedral	3.5	2.72	2.97[a]			
split (100)	3.3	2.59	2.81	3.06	3.23	2.93
Fe	Present		Ref.[74]	Ref.[75]	Ref.[75]	Ref.[76]
tetrahedral	4.2	4.31	4.16[a]			4.14
octahedral	5.0	4.78	4.19[a]			4.82
split (110)	3.9	3.79	3.53	4.11	3.65	3.64
split (111)	4.9	4.28	4.02	4.01	4.24	4.34
split (100)	4.8	4.81	4.34	4.28	4.60	4.64

[a] Calculated using parameters from the given reference.

In general, the DFT results are well reproduced or slightly underestimated by the MEAM potentials. According to the present MEAM potential, the most stable form of a self-interstitial defect for fcc Al is a dumbbell along the [100] direction, in agreement with the DFT results and an experimental observation by Jesson *et al.*[77]. The results for Mg are better than those published previously[47,73]. The present Mg potential indicates that the tetrahedral site will be most stable in agreement with the DFT calculations. For both Cu and Fe, the new MEAM potential produces the same relative stability of the examined interstitial sites with the DFT calculations.

D. Surfaces

A semi-infinite surface is one of the simplest forms of defects. To test the transferability of the new MEAM potentials, formation energies for several 1×1×7 surface slabs with 8 Å vacuum layer were computed. Eight atomic layers were used for the Si(111) surface and 12 layers for the 2×1 Si(100) surface reconstruction. The surface formation energy per unit surface area $E_{\rm surf}$ is defined as

$$E_{\rm f}^{\rm surf} = \frac{E_{\rm tot}[N] - N\varepsilon}{A}, \qquad (3)$$

where $E_{\rm tot}[N]$ is the total energy of the structure with two surfaces, N is the number of atoms in the structure, ε is the total energy per atom in the bulk, and A is the total area of both surfaces. Table IV shows the surface formation energies of several surfaces constructed from fcc Al, hcp Mg, fcc Cu, and bcc Fe crystals. Results from the present MEAM potentials agree, in the order of magnitude, with the DFT calculations, except for Fe values being underestimated.

The surfaces with lowest energy without reconstruction are identified correctly by the present MEAM potentials. The 2×1 reconstruction of the Si(100) surface leads to

TABLE IV. Surface formation energies for Al, Si, Mg, Cu, and Fe. The units are mJ/m^2. The second column indicates if the structure was relaxed. Comparisons with other classical MD (CMD), DFT, and experimental values for polycrystalline surfaces and Si facets are also given.

Surface	Rlx	DFT	MEAM	CMD		DFT	EXP
Al		Present		Ref.[11]	Ref.[49b]	Ref.[78]	Ref.[79]
(111)	No	780	820		913	1199	1143
(111)	Yes	780	752	629	912		
(110)	No	990	1154		1113	1271	
(110)	Yes	960	1135	948	1107		
(100)	No	890	1121		1012	1347	
(100)	Yes	890	1088	848	1002		
Si		Present		Ref.[80]	Ref.[81]	Ref.[82]	Ref.[83]
(111)	No	1620	1254	1405		1820	
(111)	Yes	1570	1196	1405		1740	1230
(100)	No	2140	1850	2434		2390	
(100)	Yes	2140	1743	1489		2390	
(100)	2×1		1241		2050	1450	1360
Mg	Rlx	Present		Ref.[12]	Ref.[49b]	Ref.[78]	Ref.[79]
(0001)	No	530	780		500	792	785
(0001)	Yes	530	713	310	499		
$(10\bar{1}0)$	No	850	878		629	782	
$(10\bar{1}0)$	Yes	850	859	316	618		
Cu		Present		Ref.[84b]	Ref.[62b]	Ref.[78]	Ref.[79]
(111)	No	1290	1411	1185	919	1952	1825
(111)	Yes	1290	1411	1181	903		
(110)	No	1550	1645	1427	1177	2237	
(110)	Yes	1510	1614	1412	1153		
(100)	No	1440	1654	1291	1097	2166	
(100)	Yes	1430	1653	1288	1083		
Fe		Present		Ref.[25b]	Ref.[74b]	Ref.[85]	Ref.[79]
(111)	No	2760	1366	1941	2012	2660	2475
(111)	Yes	2700	1306	1863	1998	2580	
(110)	No	2420	1378	1434	1651	2380	
(110)	Yes	2420	1372	1429	1651	2370	
(100)	No	2500	1233	1703	1790	2480	
(100)	Yes	2480	1222	1690	1785	2470	

[a] Value from the given reference.
[b] Calculated using parameters from the given reference.

symmetric dimers in accord with other Si potentials[86]. Note that surface formation energies from the present PAW GGA calculations are lower than our previously published results[47] using ultrasoft pseudopotentials within local density (LDA) approximation—it is known that GGA leads to surface energies which are 7–16% lower than LDA values for jellium and 16–29% lower than the experimental results[45,78]. A procedure[87] and new DFT functionals[88,89] were suggested to correct the errors of LDA and GGA approximations. Similar correction can be applied to vacancy formation energies[90], but such corrections were not applied in the present study.

E. Stacking faults

Using an assumption of a planar dislocation core, the Peierls-Nabarro model[91,92] is a powerful theory to quantify the dislocation core properties. In that model, a dislocation is defined by a continuous distribution of shear along the glide plane, and the restoring force acting between atoms on either sides of the interface is balanced by the resultant stress of the distribution. As shown in the recent study of Carrez *et al.*[93], a solution of the Peierls-Nabarro model can be obtained numerically by identifying the restoring force to the gradient of the generalized stacking fault energy (GSFE) curve[94]. In addition, Van Swygenhoven *et al.*[21] claimed that the nature of slip in nanocrystalline metals cannot be described in terms of an absolute value of the stacking fault energy, and a correct interpretation requires the GSFE curve, which shows the change in energy per unit area of the crystal as a function of the displacement varied on the slip plane. However, the GSFE curve is not experimentally accessible. Therefore, to model dislocation properties reliably, the GSFE curve calculated with the MEAM potential must reproduce the DFT data.

The stacking fault energy per unit area of a stacking fault $E_{\rm f}^{\rm sf}$ is defined as

$$E_{\rm f}^{\rm sf} = \frac{E_{\rm tot}[N] - N\varepsilon}{A}, \qquad (4)$$

where $E_{\rm tot}[N]$ is the total energy of the structure with a stacking fault, N is the number of atoms in the structure, ε is the total energy per atom in the bulk, and A is the total area of surface.

As a validation test of the MEAM potential, the GSFE curves obtained by molecular statics (MS) were compared with the DFT data by Zimmerman *et al.*[95] for Al and Cu, by the present authors for Fe, and by Datta *et al.*[96] for Mg. After lowering the $C_{\rm min}$ parameter to 0.8, the GSFE curves calculated by MS using the MEAM potential for Al, Cu, and Mg show the skewed sinusoidal shape in agreement with the DFT predictions (Fig. 2) illustrating reasonable agreement with the DFT GSFE curves.

IV. MEAM PARAMETERS FOR ELEMENT PAIRS

The MEAM potential parameters for each element pair were initialized to match the ab-initio heat of formation, equilibrium volume, bulk modulus, and elastic moduli in the hypothetical NaCl reference structure, which was chosen for its simplicity. Since the equilibrium volume, cohesive energy, and bulk modulus of the NaCl structure are directly related to MEAM parameters, they can be reproduced exactly. An improved agreement of the shear moduli from MEAM and ab-initio simulations was achieved in some cases by adjusting the electron density scaling factor ρ_0. Then, heat of formation of binary compounds in a variety of crystal structures from MEAM were examined and compared with the ab-initio results. To correlate the MEAM results with the lowest formation energies of the compounds from DFT calculations, the MEAM screening and $\triangle H_{\rm B1}^{\rm XY}$ parameters for element pairs were adjusted. The final MEAM parameters are given in Table V. The predicted MEAM properties for the NaCl reference structure are compared with DFT results in Table VI, and show that in general the MEAM heat of formation, bulk modulus, and equilibrium volume reproduce the DFT results well. In contrast, the shear elastic constants are not well reproduced. In fact the sign of the shear elastic constant, representing crystal stability, is frequently in disagreement with the DFT results. This is really not a significant problem as the NaCl structure does not exist in nature. A more important criteria for success of these potentials is how they perform for lower energy crystal structures. We address this issue in the next section.

A. Heat of formation for binary compounds

The alloy phases that the MEAM potential predicts as most likely to form at the temperature $T = 0$ K are those with the lowest heat of formation per atom, ΔH, which is defined as

$$\Delta H = \frac{E_{\rm tot}[N_{\rm X} + N_{\rm Y}] - N_{\rm X}\varepsilon_{\rm X} - N_{\rm Y}\varepsilon_{\rm Y}}{N_{\rm X} + N_{\rm Y}}, \qquad (5)$$

$E_{\rm tot}$ is the total energy of the simulation cell, $N_{\rm X}$ and $N_{\rm Y}$ are the numbers of type-X and type-Y atoms in the cell, $\varepsilon_{\rm X}$ and $\varepsilon_{\rm Y}$ are the total energies per atom for type-X and type-Y in their ground state bulk structures, respectively.

To check the validity of our new potentials, we computed the heat of formation per atom for many intermetallic phases of all alloy pairs. The total energy values in Eq. (5) for B1, B2, B3, C1, C15, $D0_3$, A15, $L1_2$, and other relevant structures were evaluated at the optimal atomic volume for each structure. Heat of formation for basic binary compounds based on the new MEAM potential and DFT results were calculated and compared with experimental values (Figures 3–5). The DFT and MEAM

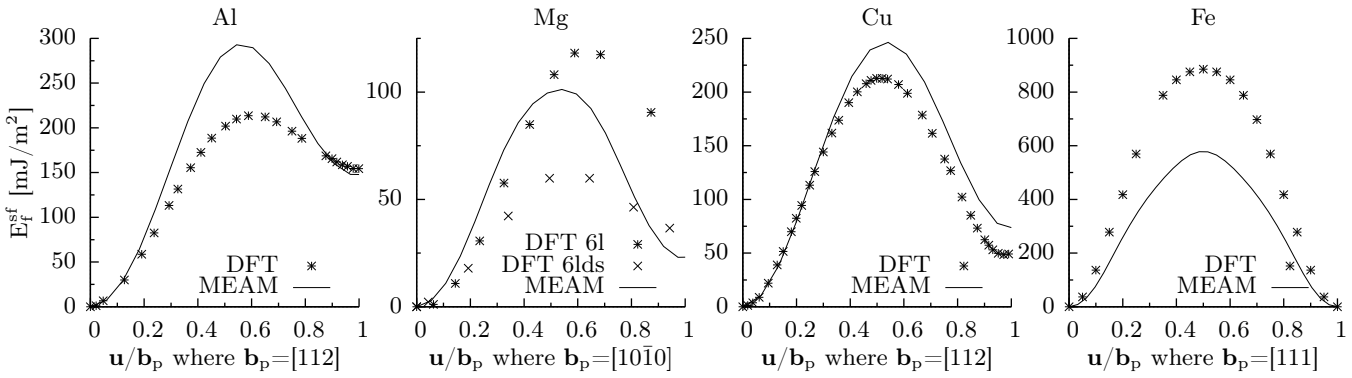

FIG. 2. GSFE curves for Al, Mg, Cu, and Fe obtained with the MEAM potential and compared with the DFT data.

TABLE V. The MEAM potential parameters for element pairs. $\triangle H_{B1}^{XY}$ is the heat of formation of the NaCl structure (reference) with the type-X and type-Y elements relative to the energies of elemental X and Y in their equilibrium reference state, r_e is their equilibrium nearest neighbor distance, α is the exponential decay factor for the universal energy, C_{max} and C_{min} are screening parameters (C^{XYX} denotes type-Y element between two type-X elements). Non-zero parameters $\delta_r = \delta_a = 0.1$ in Rose Eq. (B1–B4) were used for SiFe pair.

X	Y	$\triangle H_{B1}^{XY}$[eV]	r_e^{XY}[Å]	α^{XY}	C_{min}^{XYX}	C_{max}^{XYX}	C_{min}^{YXY}	C_{max}^{YXY}	C_{min}^{XXY}	C_{max}^{XXY}	C_{min}^{XYY}	C_{max}^{XYY}
Al	Si	0.28	2.62	4.56	0.5	2.8	2.0	2.8	2.0	2.8	2.0	2.8
Al	Mg	0.23	2.87	4.52	2.0	2.8	0.0	2.8	2.0	2.8	0.0	2.8
Al	Cu	0.19	2.53	4.65	0.0	2.8	2.0	2.8	2.0	2.8	2.0	2.8
Al	Fe	0.26	2.45	4.64	0.9	2.8	0.1	2.8	2.0	2.8	2.0	2.8
Si	Mg	0.20	2.75	4.73	1.0	2.8	1.0	2.8	2.0	2.8	2.0	2.8
Si	Cu	0.14	2.46	4.74	0.0	2.8	0.0	2.8	2.0	2.8	2.0	2.8
Si	Fe	-0.07	2.39	5.17	1.0	2.8	1.0	2.8	2.0	2.8	0.0	2.8
Mg	Cu	0.23	2.63	4.70	2.0	2.8	0.0	2.8	2.0	2.8	2.0	2.8
Mg	Fe	0.60	2.61	4.96	0.65	2.8	0.0	2.8	2.0	2.8	2.0	2.8
Cu	Fe	0.63	2.42	5.21	2.0	2.8	0.0	2.8	2.0	2.8	2.0	2.8

results for the phases with lowest ΔH are also shown in Tables VIII–IX.

The agreement between MEAM and DFT is quite satisfactory. In most cases, the MEAM results preserve the order of stability predicted by the DFT results. The differences in the heat of formation per atom from the MEAM and DFT results are less than 0.5 eV at most. In general the atomic volumes predicted by MEAM agree at least qualitatively with the DFT and experimental results. The MEAM calculations of the bulk moduli also agree semi-quantitatively with DFT and experimental results, usually within 20%. Predicted shear moduli usually follow the DFT and experimental results, but in some cases there is significant disagreement.

B. Substitutions

The formation energy of a substitutional point defect E_f^{sub}, in the case of the substitution of a type-X atom of the host with a type-Y atom, is defined by

$$E_f^{sub} = E_{tot}[(N-1)+1] - (N-1)\varepsilon_X - \varepsilon_Y \qquad (6)$$

where $E_{tot}[(N-1)+1]$ is the total energy of a system of $N-1$ host type-X atoms and one type-Y atom that replaced type-X atom in the original bulk position, ε_X and ε_Y are the total energies per atom for type-X and type-Y atoms in their ground state bulk structures. Table VII shows the results of substitutional defect calculations using the MEAM potentials and the DFT results. In general the MEAM results qualitatively agree with the DFT results. In a number of cases of small heat of formation, MEAM indicates a small heat, but of the incorrect sign. The most significant error is for Al in Si where MEAM predicts a large endothermic heat and DFT predicts a much smaller value, otherwise there is general agreement.

C. Finite temperature tests

Real life applications of MD potentials require extensive testing at finite temperatures. Basic finite temperature tests of the potentials, in accord with recommendations of Lee *et al.*[15], revealed formation of an unknown solid structure when the temperature of fcc Al crystal was

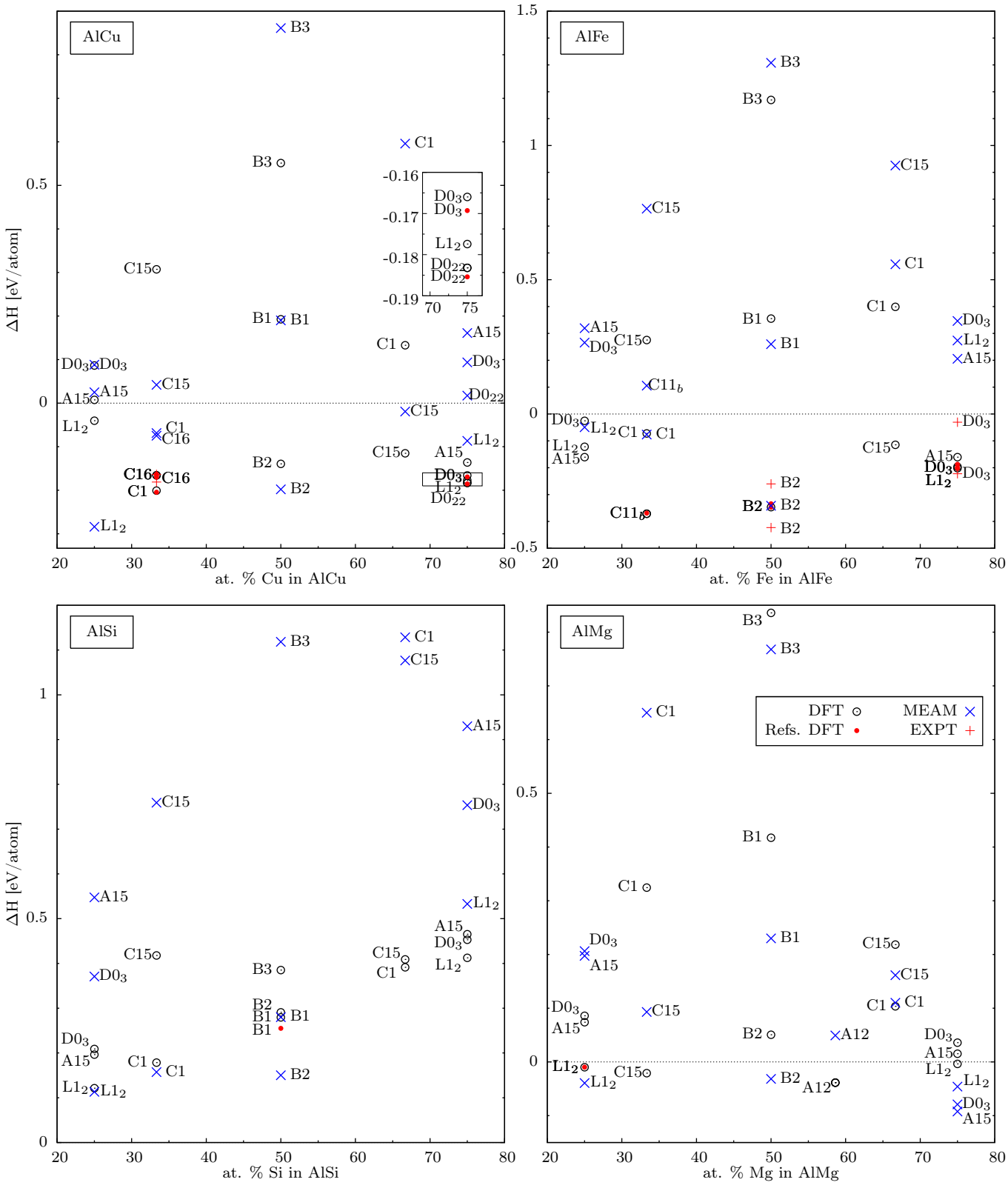

FIG. 3. (Color online) Heat of formation of AlSi, AlMg, AlCu, AlFe binary compounds from MEAM, DFT, and experiments. References: AlSi[6], AlMg[97], AlCu[98–101], AlFe[102–104]. DFT points are labeled on the left, MEAM and experimental on the right. Values for the most stable compounds are also shown in Table VIII. The inside plot is a magnified portion of a larger plot.

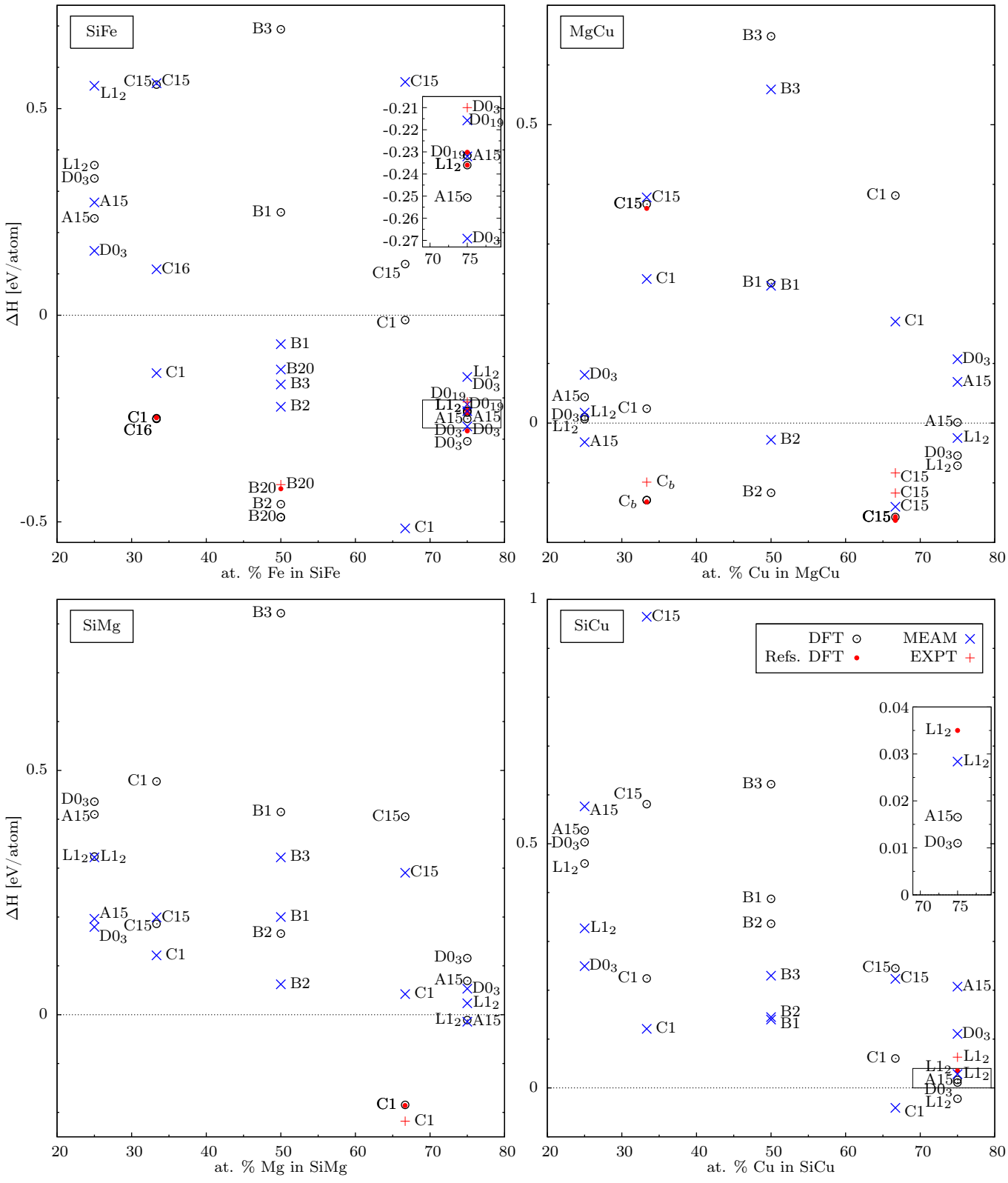

FIG. 4. (Color online) Heat of formation of SiMg, SiCu, SiFe, MgCu binary compounds from MEAM, DFT, and experiments. References: SiMg[101], SiCu[105,106], SiFe[97,107], and MgCu[97,108]. DFT points are labeled on the left, MEAM and experimental on the right. Values for the most stable compounds are also shown in Table IX. The inside plot is a magnified portion of a larger plot.

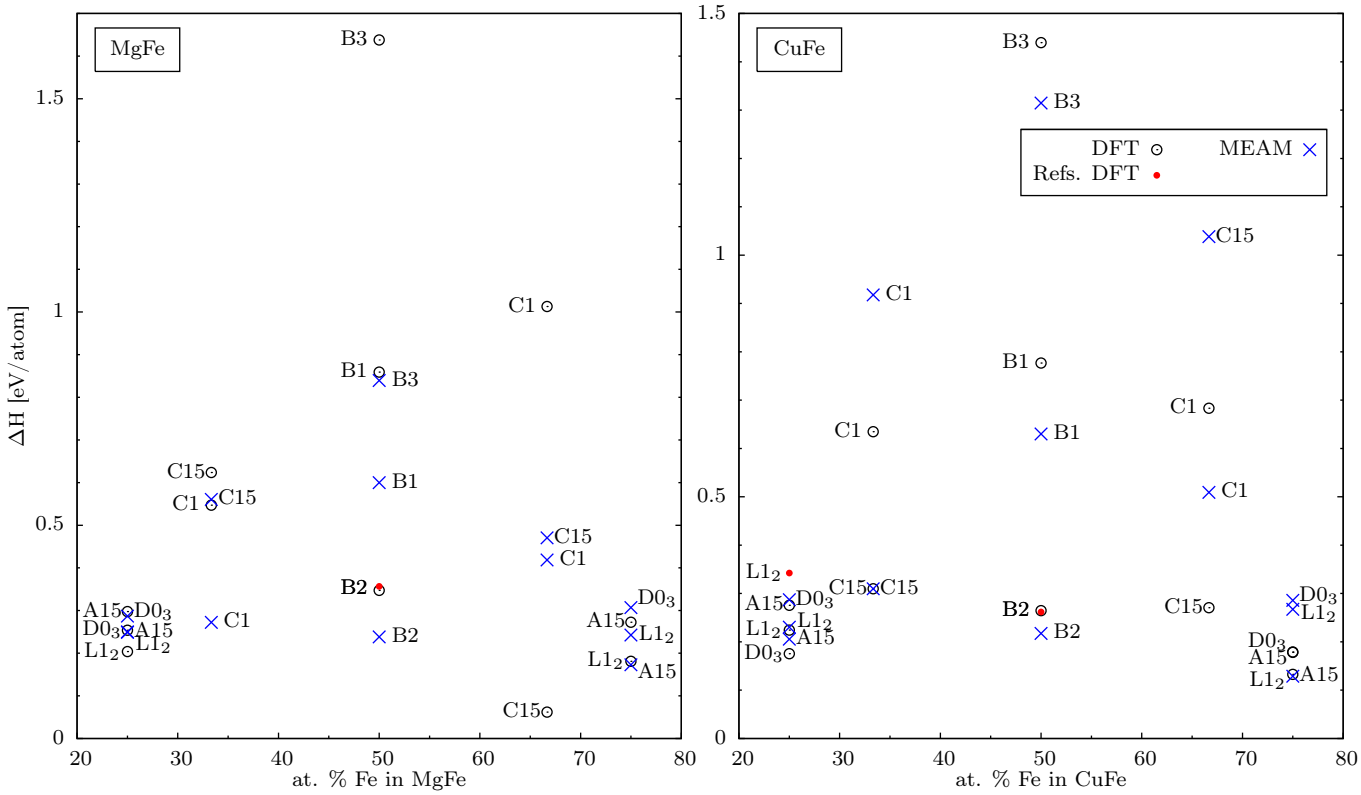

FIG. 5. (Color online) Heat of formation of MgFe and CuFe binary compounds from MEAM and DFT. References: MgFe[97], CuFe[97]. DFT points are labeled on the left, MEAM on the right. Values for the most stable compounds are also shown in Table IX.

TABLE VI. Structural and elastic properties of element pairs in the reference NaCl (B1) crystal structure from DFT and MEAM calculations. ΔH is the heat of formation in eV/atom, V_0 is the volume per atom in Å^3. Elastic constants B_0, C_{44}, and $(C_{11}-C_{12})/2$ are in GPa.

pair	method	ΔH	V_0	B_0	C_{44}	$\frac{C_{11}-C_{12}}{2}$
AlSi	DFT	0.28	17.9	76.7	10	76
	MEAM	0.28	18.0	76.4	-13	8
AlMg	DFT	0.42	23.7	30.9	-18	36
	MEAM	0.23	23.6	33.9	-3	35
AlCu	DFT	0.19	16.1	77.5	-18	52
	MEAM	0.19	16.2	77.4	-19	56
AlFe	DFT	0.36	14.7	90.3	-25	105
	MEAM	0.26	14.7	92.7	-27	109
SiMg	DFT	0.41	20.9	50.6	-26	48
	MEAM	0.20	20.8	54.9	9	61
SiCu	DFT	0.39	14.9	99.0	-29	58
	MEAM	0.14	14.9	105.9	9	223
SiFe	DFT	0.25	12.9	100.9	-70	112
	MEAM	-0.07	13.7	157.9	65	363
MgCu	DFT	0.23	18.5	48.7	-10	49
	MEAM	0.23	18.2	49.6	-1	61
MgFe	DFT	0.86	17.7	50.4	-23	83
	MEAM	0.60	17.8	56.5	-17	62
CuFe	DFT	0.78	14.1	107.4	-23	134
	MEAM	0.63	14.2	111.8	10	131

TABLE VII. The formation energies of substitutional point defects in Al, Si, Mg, Cu, and Fe. All energy values are given in eV. DFT values are given in parentheses.

Host	Substitute atom				
	Al	Si	Mg	Cu	Fe
Al		0.5 (0.5)	−0.2 (0.05)	−1.1 (−0.1)	−1.3 (−0.4)
Si	7.0 (0.9)		2.9 (2.4)	1.9 (2.)	1.6 (1.9)
Mg	−0.7 (0.06)	0.2 (0.4)		−0.2 (0.2)	1.5 (1.1)
Cu	0.7 (−0.7)	0.8 (−0.2)	1.1 (−0.2)		2.9 (1.4)
Fe	0.2 (−0.7)	−2.9 (−1.1)	0.8 (1.0)	−0.3 (0.8)	

increased to 800 K under zero pressure conditions. To prevent formation of this structure, $\beta^{(1)}$ and $t^{(1)}$ parameters of Al were adjusted. Heating of other elements under zero pressure conditions did not result in forming new structures.

To test a system including all components of the new potential, an 20–100 °C average thermal expansion coefficient of a model system with the composition similar to AA 6061 alloy (Table X) was evaluated and compared with experimental data. Atoms of constituents were placed in the substitutional positions of a 20x20x20 fcc Al cell. The system was heated from -200 °C to 20 °C (and 100 °C) over the interval of 0.1 ns, and then equilibrated at 20 °C

TABLE VIII. Structural and elastic properties of element pairs in varying crystal structures from the present DFT and MEAM calculations compared with references and measured values. ΔH is the heat of formation in meV/atom, V_0 is the volume per atom in Å^3, and elastic constants B_0, C_{44}, and $(C_{11}-C_{12})/2$ are in GPa.

compos.	str.	met.	ΔH	V_0	B_0	C_{44}	$\frac{C_{11}-C_{12}}{2}$
Al_3Si	$L1_2$	DFT	121	16.04	74.3	24.1	9.4
		MEAM/EAM	113	16.67	96.7	31.2	31.2
Al_2Si	C1	DFT	178	18.78	62.9	25.4	−11.8
		MEAM/EAM	157	19.17	73.6	15.3	0.0
AlSi	B2	DFT	291	15.91	78.8	22.4	−32.8
		MEAM/EAM	150	16.25	102.1	29.1	−17.0
$Al_{12}Mg_{17}$	A12	DFT	−39, −35[109], −37[110], −48[111]	20.12, 18.65[109], 20.04[110], 20.25[111]	50.1, 49.6[111]	20.0[111]	28.9[111]
		MEAM/EAM	49, −19[112], −36[113]	21.28, 20.30[112]	49.6[112]	11.5[112]	23.9[112]
		EXP	−34[114]	20.13[115], 20.30[116]			
Al_3Mg	$L1_2$	DFT	−10, −15[109], −9[27]	17.80, 16.52[109], 17.78[27]	63.3	35.3	31.9
		MEAM/EAM	−39, −2[27]	19.04, 17.54[27]	62.7	33.3	14.7
$AlMg_3$	$L1_2$	DFT	−4, −5[109], −3[27]	20.98, 19.18[109], 19.89[27]	43.9	25.2	22.6
		MEAM/EAM	−46, 21[27]	21.99, 20.98[27]	45.0	24.9	13.8
AlMg	B2	DFT	51, 50[109], 51[109]	19.50, 18.00[109], 19.48[109]	47.9	38.4	−7.5
		MEAM/EAM	−32, 90[109]	20.29, 19.57[109]	50.6	32.9	8.9
Al_2Cu	C16	DFT	−166, −170[97], −166[101], −163[98]	14.95, 14.89[98]	96.3		
		MEAM/EAM	−75	15.80			
		EXP	−161[117]	14.90[98]			
	C1	DFT	−201, −202[98], −204[97]	16.14, 16.12[98]	93.1	81.6	46.0
		MEAM/EAM	−69	17.31	77.4	43.2	7.7
		EXP		15.63[98]			
$AlCu_3$	$D0_{22}$	DFT	−183, −185[97]	12.52	128.1		
		MEAM/EAM	17	13.08			
	$L1_2$	DFT	−177, −219[118]	12.59	128.4	81.1	13.8
		MEAM/EAM	−87, −229[118]	13.47	131.9	72.4	26.8
	$D0_3$	DFT	−166, −169[97]	12.60	127.9	98.4	1.1
		MEAM/EAM	94	12.34	107.8	88.7	4.9
	A15	DFT	−136	12.77	124.7	34.5	102.8
		MEAM/EAM	161	13.48	111.6	200.5	92.8
Al_3Cu	$L1_2$	DFT	−40	15.22	89.9	23.4	61.5
		MEAM/EAM	−284	14.58	106.0	40.3	41.2
AlCu	B2	DFT	−139	13.45	108.6	31.4	−15.4
		MEAM/EAM	−198	14.15	109.2	56.7	2.8
AlFe	B2	DFT	−347, −347[97], −334[119], −379[120], −420[121], −400[122], −338[123], −311[124], −1500[103]	11.86, 11.88[119], 12.07[120], 11.33[125], 11.22[121], 11.65[122], 11.89[123], 11.93[124], 12.19[103]	174.6, 177.0[119], 183.0[125], 155.0[124], 156.0[103]	138.8, 165.0[125], 107.0[103]	61.8, 80.0[125], 38.1[103]
		MEAM/EAM	−342, −298[126], −260[102], −106[127]	12.88, 12.32[128], 13.92[127], 11.45[104]	145.3, 144.0[128], 138.0[127], 193.0[104]	111.7, 117.0[128], 110.7[127]	79.6, 18.0[128], 7.9[127]
		EXP	−260[129], −423[130], −250[131], −280[132]	12.23[133]	152.0[134], 136.0[135]	127.0[134], 127.1[135]	43.0[134], 33.7[135]
$AlFe_3$	$D0_3$	DFT	−202, −203[97], −200[119], −221[120], −230[121], −202[123], −201[124], −1860[103]	11.79, 11.81[119], 12.01[120], 14.65[121], 11.82[123], 12.09[124], 11.57[103]	160.0, 174.0[119], 151.0[124], 170.0[103]	140.0, 137.5[103]	25.5, 10.8[103]
		MEAM/EAM	346, −206[126], −222[102], −74[127]	12.01, 11.77[102], 12.86[127], 10.80[104]	137.5, 146.0[127], 229.0[104]	129.0, 162.0[102], 126.3[127]	30.0, 53.0[102], 12.6[127]
		EXP	−202[131], −321[130]	12.07[133]	144.0[135]	131.7[135]	20.2[135]
	$L1_2$	DFT	−196, −187[97], −200[119], −40[121], −222[124]	12.13, 12.14[119], 14.14[121], 12.35[124]	166.3, 158.0[119], 168.0[124]	125.1	11.5
		MEAM/EAM	274, −180[126]	12.88	139.5	96.9	84.0
	A15	DFT	−161	12.08	156.9	67.3	135.1
		MEAM/EAM	205	12.59	166.7	35.5	153.5
$AlFe_2$	C15	DFT	−115, −60[121]	12.42, 11.43[121]	130.2	55.0	52.2
		MEAM/EAM	925	13.67	127.8	259.2	551.0
Al_3Fe	A15	DFT	−161	13.91	121.5	67.7	120.0
		MEAM/EAM	321	15.03	103.5	1.8	66.6
	$L1_2$	DFT	−122, −150[121], −105[124]	13.68, 13.07[121], 13.69[124]	126.5, 98.8[124]	85.9	49.9
		MEAM/EAM	−49	14.83	108.5	59.4	20.3
	$D0_3$	DFT	−25, −99[120], −13[124]	13.38, 13.57[120], 13.35[124]	126.0, 119.6[124]	91.4	−48.3
		MEAM/EAM	266	14.81	93.8	57.7	−31.1
Al_2Fe	$C11_b$	DFT	−371, −420[121]	12.78, 12.35[121], 12.80[136]	149.0		
		MEAM/EAM	106	14.71			
	C1	DFT	−72	15.25	98.6	76.8	55.0
		MEAM/EAM	−76	16.12	90.4	47.5	36.4

TABLE IX. Structural and elastic properties of element pairs in varying crystal structures from the present DFT and MEAM calculations compared with references and measured values. ΔH is the heat of formation in meV/atom, V_0 is the volume per atom in Å^3, and elastic constants B_0, C_{44}, and $(C_{11}-C_{12})/2$ are in GPa.

compos.	str.	met.	ΔH	V_0	B_0	C_{44}	$\frac{C_{11}-C_{12}}{2}$
$SiMg_2$	C1	DFT	-185, -186[101]	21.41	54.1	47.6	47.3
		MEAM/EAM	42	23.05	47.8	20.9	32.2
		EXP	-225[117]				
$SiMg_3$	$L1_2$	DFT	-11	19.29	50.8	29.9	37.1
		MEAM/EAM	24	20.70	57.5	23.5	21.8
	A15	DFT	69	20.09	44.1	9.3	31.8
		MEAM/EAM	-14	21.25	56.3	32.2	33.9
$SiCu_3$	$L1_2$	DFT	-22, 35[106]	12.18	137.3	65.0	38.1
		MEAM/EAM	28	13.37	134.9	64.4	33.0
		EXP	63[105]				
$SiCu_2$	C1	DFT	60	14.26	111.9	76.3	23.1
		MEAM/EAM	-41	14.81	102.8	97.9	16.2
SiFe	B20	DFT	-489, -484[97], -420[107]	11.04	226.5		
		MEAM/EAM	-132	13.11			
		EXP	-410[107]				
	B2	DFT	-457	10.55	231.9	87.0	155.8
		MEAM/EAM	-222	13.09	177.7	36.2	225.3
$SiFe_3$	$D0_3$	DFT	-305, -315[97], -280[107]	10.99	204.5	142.4	54.5
		MEAM/EAM	-269	12.03	169.2	91.6	36.6
		EXP	-210[107]				
	A15	DFT	-251	11.44	173.3	72.3	125.3
		MEAM/EAM	-232	12.28	190.1	47.6	119.9
	$L1_2$	DFT	-236, -236[97]	11.38	188.4	116.0	26.6
		MEAM/EAM	-149	11.80	188.6	65.1	135.8
	$D0_{19}$	DFT	-232, -230[97]	11.28	160.1		
		MEAM/EAM	-216	12.05			
Si_2Fe	C1	DFT	-249, -248[97]	13.05	169.4	136.8	15.5
		MEAM/EAM	-140	15.53	158.7	95.7	41.3
	C16	DFT	-251, -248[97]	12.39	170.6		
		MEAM/EAM	111	13.64			
$SiFe_2$	C1	DFT	-12	12.95	159.6	82.6	-1.4
		MEAM/EAM	-516	12.95	182.4	154.6	226.8
Mg_2Cu	C_b	DFT	-129, -131[97], -132[137], -137[108]	18.13	57.1		
		EXP	-99[138]				
$MgCu_2$	C15	DFT	-157, -160[97], -163[108], -157[137]	14.58	90.6	45.4	25.2
		MEAM/EAM	-140	14.50	104.7	21.5	-12.0
		EXP	-117[138], -83[139]				
MgCu	B2	DFT	-117	15.65	69.3	60.3	16.9
		MEAM/EAM	-28	15.56	73.6	51.1	-11.6
$MgCu_3$	$L1_2$	DFT	-71	13.49	96.6	62.6	21.5
		MEAM/EAM	-25	13.81	103.9	42.5	29.0
	$D0_3$	DFT	-54	13.52	96.5	75.2	0.3
		MEAM/EAM	107	13.43	95.7	64.1	-22.4
$MgFe_2$	C15	DFT	62	13.58	91.4	72.0	53.4
		MEAM/EAM	471	14.79	95.8	322.9	605.7
$MgFe_3$	$L1_2$	DFT	181	13.11	122.6	96.9	14.0
		MEAM/EAM	243	13.65	116.4	64.5	45.5
Mg_3Fe	$L1_2$	DFT	204	18.29	51.6	52.1	18.9
		MEAM/EAM	249	19.08	54.5	30.0	23.1
MgFe	B2	DFT	347, 357[97]	15.39	71.4	68.7	-25.4
		MEAM/EAM	238	15.82	86.4	63.2	13.7
$CuFe_3$	$L1_2$	DFT	133	11.73	132.5	99.9	6.8
		MEAM/EAM	267	11.78	172.6	80.5	68.0
	A15	DFT	178	11.95	137.6	54.2	134.7
		MEAM/EAM	129	12.26	192.3	70.5	155.2
Cu_3Fe	$D0_3$	DFT	175	12.10	139.2	105.5	-2.0
		MEAM/EAM	287	11.59	134.0	130.8	20.7
	$L1_2$	DFT	224, 342[97]	12.16	135.2	60.7	-0.0
		MEAM/EAM	230	12.01	153.2	66.7	71.7
CuFe	B2	DFT	264, 262[97]	11.88	211.4	108.7	-52.0
		MEAM/EAM	217	12.10	161.7	105.6	45.7

TABLE X. Composition limits of AA 6061 alloy[140] and a model system used to estimate thermal expansion coefficient.

Element	Limits		Model [wt. %]
	low [wt. %]	high [wt. %]	
Si	0.40	0.8	0.51
Mg	0.8	1.2	1.00
Cu	0.15	0.40	0.30
Fe	no	0.7	0.50
Mn	no	0.15	0.00
Cr	0.04	0.35	0.00
Zn	no	0.25	0.00
Ti	no	0.15	0.00

TABLE XI. Thermal expansion coefficient of single crystal Al and AA 6061 alloy between 20°C and 100°C in the units of μm/m/K.

	CMD		Exp	
	present	Ref.[141]	Ref.[142]	Ref.[140]
Al fcc	14.4	15-25	25.4	23.6
AA 6061	14.6			23.6

(and 100 °C) for 1 ns under zero pressure conditions. Table XI shows the values of 20–100 °C average thermal expansion coefficients. The MEAM result for single crystal Al is in the lower range of other MD potentials and experiments. Since Al is a dominant element of the AA 6061 alloy, the thermal expansion coefficient for alloy is similarly underestimated, possibly also due to imperfections of the structure of the real material.

V. CONCLUSIONS

In this study we developed MEAM potentials for the pair combinations of aluminum, silicon, magnesium, copper, and iron. The MEAM formalism allows any of these potentials to be combined to enable prediction of multi-component alloy properties. These potentials reproduce a large body of elemental and binary properties from DFT calculations at the temperature of 0 K and experimental results. Basic finite temperature tests of the single element potentials and their alloy combinations were also performed. With focus to facilitate reproducibility of the presented results[42], and subject to further testing and improvements, these potentials are one step towards designing multi-component alloys by simulations.

ACKNOWLEDGMENT

The authors are grateful to the Center for Advanced Vehicular Systems at Mississippi State University for supporting this study. Computer time allocation has been provided by the High Performance Computing Collaboratory (HPC^2) at Mississippi State University. Computational package LAMMPS[143] with ASE[144] interface was used to perform MD simulations. Much appreciated tests of the new MEAM potentials, including the high temperature simulations of Al that revealed formation of unknown Al phase at 800 K, were performed by Chandler Becker and Tanner Hamann at the Metallurgy Division of the Material Measurement Laboratory, National Institute of Standards and Technology (NIST). Comparison of ab-initio elastic constants and related discussion with Hannes Schweiger from Materials Design are also appreciated. Classical MD potentials from other authors examined in this study were downloaded from the Interatomic Potentials Repository Project database[145].

Sandia National Laboratories is a multi-program laboratory managed and operated by Sandia Corporation, a wholly owned subsidiary of Lockheed Martin Corporation, for the U.S. Department of Energy's National Nuclear Security Administration under contract DE-AC04-94AL85000.

Appendix A: MEAM theory

The total energy E of a system of atoms in the MEAM[4] is approximated as the sum of the atomic energies

$$E = \sum_i E_i. \tag{A1}$$

The energy of atom i consists of the embedding energy and the pair potential terms:

$$E_i = F_i\left(\bar{\rho}_i\right) + \frac{1}{2}\sum_{j\neq i}\phi_{ij}\left(r_{ij}\right). \tag{A2}$$

F is the embedding function, $\bar{\rho}_i$ is the background electron density at the site of atom i, and $\phi_{ij}\left(r_{ij}\right)$ is the pair potential between atoms i and j separated by a distance r_{ij}. The embedding energy $F_i\left(\bar{\rho}_i\right)$ represents the energy cost to insert atom i at a site where the background electron density is $\bar{\rho}_i$. The embedding energy is given in the form

$$F_i\left(\bar{\rho}_i\right) = \begin{cases} A_i E_i^0 \bar{\rho}_i \ln\left(\bar{\rho}_i\right) & \text{if } \bar{\rho}_i \geq 0, \\ -A_i E_i^0 \bar{\rho}_i & \text{if } \bar{\rho}_i < 0, \end{cases} \tag{A3}$$

where the sublimation energy E_i^0 and parameter A_i depend on the element type of atom i. The background electron density $\bar{\rho}_i$ is given by

$$\bar{\rho}_i = \frac{\rho_i^{(0)}}{\rho_i^0} G\left(\Gamma_i\right), \tag{A4}$$

where

$$\Gamma_i = \sum_{k=1}^{3} t_i^{(k)} \left(\frac{\rho_i^{(k)}}{\rho_i^{(0)}}\right)^2 \tag{A5}$$

and

$$G\left(\Gamma\right) = \begin{cases} \sqrt{1+\Gamma} & \text{if } \Gamma \geq -1, \\ -\sqrt{\left|1+\Gamma\right|} & \text{if } \Gamma < -1. \end{cases} \tag{A6}$$

The zeroth and higher order densities, $\rho_i^{(0)}$, $\rho_i^{(1)}$, $\rho_i^{(2)}$, and $\rho_i^{(3)}$ are given in Eqs. (A9). The composition-dependent electron density scaling ρ_i^0 is given by

$$\rho_i^0 = \rho_{i0} Z_{i0} G\left(\Gamma_i^{\text{ref}}\right), \tag{A7}$$

where ρ_{i0} is an element-dependent density scaling, Z_{i0} is the first nearest-neighbor coordination of the reference system, and Γ_i^{ref} is given by

$$\Gamma_i^{\text{ref}} = \frac{1}{Z_{i0}^2} \sum_{k=1}^{3} t_i^{(k)} s_i^{(k)}, \tag{A8}$$

where $s_i^{(k)}$ is the shape factor that depends on the reference structure for atom i. Shape factors for various structures are specified in the work of Baskes[4]. The partial electron densities are given by

$$\rho_i^{(0)} = \sum_{j \neq i} \rho_j^{a(0)}\left(r_{ij}\right) S_{ij} \tag{A9a}$$

$$\left(\rho_i^{(1)}\right)^2 = \sum_{\alpha} \left[\sum_{j \neq i} \rho_j^{a(1)} \frac{r_{ij\alpha}}{r_{ij}} S_{ij}\right]^2 \tag{A9b}$$

$$\left(\rho_i^{(2)}\right)^2 = \sum_{\alpha,\beta} \left[\sum_{j \neq i} \rho_j^{a(2)} \frac{r_{ij\alpha} r_{ij\beta}}{r_{ij}^2} S_{ij}\right]^2 - \frac{1}{3}\left[\sum_{j \neq i} \rho_j^{a(2)}\left(r_{ij}\right) S_{ij}\right]^2 \tag{A9c}$$

$$\left(\rho_i^{(3)}\right)^2 = \sum_{\alpha,\beta,\gamma} \left[\sum_{j \neq i} \rho_j^{a(3)} \frac{r_{ij\alpha} r_{ij\beta} r_{ij\gamma}}{r_{ij}^3} S_{ij}\right]^2 - \frac{3}{5} \sum_{\alpha} \left[\sum_{j \neq i} \rho_j^{a(3)} \frac{r_{ij\alpha}}{r_{ij}} S_{ij}\right]^2, \tag{A9d}$$

where $r_{ij\alpha}$ is the α component of the displacement vector from atom i to atom j. S_{ij} is the screening function between atoms i and j and is defined in Eqs. (A16). The atomic electron densities are computed as

$$\rho_i^{a(k)}\left(r_{ij}\right) = \rho_{i0} \exp\left[-\beta_i^{(k)}\left(\frac{r_{ij}}{r_i^0} - 1\right)\right], \tag{A10}$$

where r_i^0 is the nearest-neighbor distance in the single-element reference structure and $\beta_i^{(k)}$ is element-dependent parameter. Finally, the average weighting factors are given by

$$t_i^{(k)} = \frac{\sum_{j \neq i} t_{0,j}^{(k)} \rho_j^{a(0)} S_{ij}}{\sum_{j \neq i} \left(t_{0,j}^{(k)}\right)^2 \rho_j^{a(0)} S_{ij}}, \tag{A11}$$

where $t_{0,j}^{(k)}$ is an element-dependent parameter.

The pair potential is given by

$$\phi_{ij}\left(r_{ij}\right) = \bar{\phi}_{ij}\left(r_{ij}\right) S_{ij} \tag{A12}$$

$$\bar{\phi}_{ij}\left(r_{ij}\right) = \frac{1}{Z_{ij}}\left[2E_{ij}^u\left(r_{ij}\right) - F_i\left(\frac{Z_{ij}}{Z_i}\rho_j^{a(0)}\left(r_{ij}\right)\right) - F_j\left(\frac{Z_{ij}}{Z_j}\rho_j^{a(0)}\left(r_{ij}\right)\right)\right] \tag{A13}$$

$$E_{ij}^u\left(r_{ij}\right) = -E_{ij}\left(1 + a_{ij}^*\left(r_{ij}\right)\right) e^{-a_{ij}^*\left(r_{ij}\right)} \tag{A14}$$

$$a_{ij}^* = \alpha_{ij}\left(\frac{r_{ij}}{r_{ij}^0} - 1\right), \tag{A15}$$

where E_{ij}, α_{ij} and r_{ij}^0 are element-dependent parameters and Z_{ij} depends upon the structure of the reference system. The background densities $\hat{\rho}_i(r_{ij})$ in Eq. (A13) are the densities for the reference structure computed with interatomic spacing r_{ij}.

The screening function S_{ij} is designed so that $S_{ij} = 1$ if atoms i and j are unscreened and within the cutoff radius r_c, and $S_{ij} = 0$ if they are completely screened or outside the cutoff radius. It varies smoothly between 0 and 1 for partial screening. The total screening function is the product of a radial cutoff function and three body terms involving all other atoms in the system:

$$S_{ij} = \bar{S}_{ij} f_c\left(\frac{r_c - r_{ij}}{\Delta r}\right) \tag{A16a}$$

$$\bar{S}_{ij} = \prod_{k \neq i,j} S_{ikj} \tag{A16b}$$

$$S_{ikj} = f_c\left(\frac{C_{ikj} - C_{\min,ikj}}{C_{\max,ikj} - C_{\min,ikj}}\right) \tag{A16c}$$

$$C_{ikj} = 1 + 2\frac{r_{ij}^2 r_{ik}^2 + r_{ij}^2 r_{jk}^2 - r_{ij}^4}{r_{ij}^4 - \left(r_{ik}^2 - r_{jk}^2\right)^2} \tag{A16d}$$

$$f_c\left(x\right) = \begin{cases} 1 & x \geq 1 \\ \left[1 - \left(1-x\right)^4\right]^2 & 0 < x < 1 \\ 0 & x \leq 0 \end{cases} \tag{A16e}$$

Note that $C_{\min}$ and $C_{\max}$ can be defined separately for each *i*-*j*-*k* triplet, based on their element types. The parameter Δr controls the distance over which the radial cutoff is smoothed from 1 to 0 near $r = r_c$.

Appendix B: Equilibrium lattice parameter and bulk modulus

MEAM postulates the Rose universal equation of state[146]

$$E_{\text{R}}(a^*) = -E_{\text{c}}\left(1 + a^* + \delta\frac{\alpha a^{*3}}{\alpha + a^*}\right) e^{-a^*} \tag{B1}$$

for the reference structure of each single element and for each element pair. The a^*, scaled distance from the

equilibrium nearest neighbor position r_0, is

$$a^* = \alpha(r/r_0 - 1). \tag{B2}$$

Two δ parameters may be specified for each element/pair: δ_r for negative, and δ_a for positive a^*. Then

$$\delta = \begin{cases} \delta_r & \text{for } a^* < 0 \\ \delta_a & \text{for } a^* \geq 0. \end{cases} \tag{B3}$$

The MEAM potential parameter α is related to the equilibrium atomic volume Ω_0, the bulk modulus B_0, and the cohesive energy of the reference structure E_c as follows

$$\alpha = \sqrt{\frac{9B_0\Omega_0}{E_c}}. \tag{B4}$$

The DFT equilibrium energies and bulk moduli were obtained by fitting energy-volume dependence to Murnaghan equation of state[147]

$$E(V) = E(V_0) + \frac{B_0 V}{B_0'(B_0'-1)}\left[B_0'\left(1-\frac{V_0}{V}\right) + \left(\frac{V_0}{V}\right)^{B_0'} - 1\right]. \tag{B5}$$

Appendix C: Trigonal and tetragonal shear modulus

For small deformations of a cubic crystal, the change of energy density due to straining is

$$\triangle E_V = \frac{1}{2}C_{11}\left(\epsilon_1^2+\epsilon_2^2+\epsilon_3^2\right) + C_{12}\left(\epsilon_1\epsilon_2+\epsilon_2\epsilon_3+\epsilon_3\epsilon_1\right) + \frac{1}{2}C_{44}\left(\epsilon_4^2+\epsilon_5^2+\epsilon_6^2\right) + O(\epsilon_i^3), \tag{C1}$$

where ϵ_i are strains in modified Voigt notation.

The trigonal shear modulus C_{44} was determined from rhombohedral deformation given by $\epsilon_1 = \epsilon_2 = \epsilon_3 = 0$ and $\epsilon_4 = \epsilon_5 = \epsilon_6 = \delta$ in C1, leading to

$$\triangle E_V(\delta) = \frac{3}{2}C_{44}\delta^2 + O(\delta^3). \tag{C2}$$

The tetragonal shear modulus $(C_{11}-C_{12})/2$ was determined from the deformation given by $\epsilon_1 = \delta, \epsilon_2 = \frac{1}{1+\delta} - 1$ in C1, leading to

$$\triangle E_V(\delta) = (C_{11}-C_{12})\,\delta^2 + O(\delta^3). \tag{C3}$$

The C2 and C3 were used to estimate tetragonal and trigonal shear moduli.

* Presently at Institute of Mechanics and Fluid Dynamics, TU Bergakademie Freiberg, Lampadiusstr. 4, 09596 Freiberg, Germany

† Also at Department of Mechanical Engineering, Mississippi State University, Mississippi State, MS 39762

‡ Also at Center for Computational Sciences, Mississippi State University, Mississippi State, MS 39762

§ Also at Los Alamos National Laboratory, MST-8, MS G755, Los Alamos, NM 87545

[1] M. F. Horstemeyer, in *Pract. Aspects Comput. Chem.*, edited by J. Leszczynski and M. K. Shukla (Springer Netherlands, 2010) pp. 87–135.

[2] M. S. Daw and M. I. Baskes, Phys. Rev. Lett. **50**, 1285 (1983); Phys. Rev. B **29**, 6443 (1984); M. I. Baskes, Phys. Rev. Lett. **59**, 2666 (1987); M. S. Daw, Phys. Rev. B **39**, 7441 (1989).

[3] M. I. Baskes, J. S. Nelson, and A. F. Wright, Phys. Rev. B **40**, 6085 (1989).

[4] M. I. Baskes, Phys. Rev. B **46**, 2727 (1992).

[5] M. I. Baskes, J. E. Angelo, and C. L. Bisson, Modell. Simul. Mater. Sci. Eng. **2**, 505 (1994).

[6] K. Gall, M. F. Horstemeyer, M. van Schilfgaarde, and M. I. Baskes, J. Mech. Phys. Solids. **48**, 2183 (2000).

[7] B.-J. Lee and M. I. Baskes, Phys. Rev. B **62**, 8564 (2000).

[8] H. Huang, N. M. Ghoniem, J. K. Wong, and M. I. Baskes, Modell. Simul. Mater. Sci. Eng. **3**, 615 (1995).

[9] M. I. Baskes, Mater. Chem. Phys. **50**, 152 (1997).

[10] M. I. Baskes, Mater. Sci. Eng. A **261**, 165 (1999).

[11] B.-J. Lee, J.-H. Shim, and M. I. Baskes, Phys. Rev. B **68**, 144112 (2003).

[12] W. Hu, B. Zhang, B. Huang, F. Gao, and D. J. Bacon, J. Phys.: Condens. Matter **13**, 1193 (2001).

[13] W. Hu, H. Deng, X. Yuan, and M. Fukumoto, Eur. Phys. J. B **34**, 429 (2003).

[14] B.-J. Lee and J. W. Lee, Calphad **29**, 7 (2005).

[15] B.-J. Lee, W.-S. Ko, H.-K. Kim, and E.-H. Kim, Calphad **34**, 510 (2010).

[16] K. Kang and W. Cai, Philos. Mag. **87**, 2169 (2007).

[17] T. S. Gates, G. M. Odegard, S. J. V. Frankland, and T. C. Clancy, Compos. Sci. Technol. **65**, 2416 (2005).

[18] S. J. Noronha and D. Farkas, Phys. Rev. B **66**, 132103 (2002).

[19] E. Martínez, J. Marian, A. Arsensil, M. Victoria, and J. Perlado, J. Mech. Phys. Solids. **56**, 869 (2008).

[20] G. P. Potirniche, M. F. Horstemeyer, G. J. Wagner, and P. M. Gullett, Int. J. Plast. **22**, 257 (2006).

[21] H. Van Swygenhoven, P. M. Derlet, and A. G. Frøseth, Nat. Mater. **3**, 399 (2004).

[22] R. A. Johnson and D. J. Oh, J. Mater. Res. **4**, 1195 (1989).

[23] R. A. Johnson, Phys. Rev. B **39**, 12554 (1989).

[24] X. W. Zhou, H. N. G. Wadley, R. A. Johnson, D. J. Larson, N. Tabat, A. Cerezo, A. K. Petford-Long, G. D. W. Smith, P. H. Clifton, R. L. Martens, and T. F. Kelly, Acta Mater. **49**, 4005 (2001).

[25] X. W. Zhou, R. A. Johnson, and H. N. G. Wadley, Phys. Rev. B **69**, 144113 (2004).

[26] Y. Mishin, M. J. Mehl, and D. A. Papaconstantopoulos, Acta Mater. **53**, 4029 (2005).

[27] M. I. Mendelev, M. Asta, M. J. Rahman, and J. J. Hoyt, Philos. Mag. **89**, 3269 (2009).

[28] X. Y. Liu and J. B. Adams, Acta Mater. **46**, 3467 (1998).

[29] F. Apostol and Y. Mishin, Phys. Rev. B **83**, 054116 (2011).

[30] X.-Y. Liu, C.-L. Liu, and L. J. Borucki, Acta Mater. **47**, 3227 (1999).

[31] M. I. Mendelev, D. J. Srolovitz, G. J. Ackland, and S. Han, J. Mater. Res. **20**, 208 (2005).
[32] T. Ohira, Y. Inoue, K. Murata, and J. Murayama, Appl. Surf. Sci. **171**, 175 (2001); T. Ohira and Y. Inoue, in *MRS Proceedings*, Vol. 492 (1997) pp. 401–406.
[33] S. M. Valone, M. I. Baskes, and R. L. Martin, Phys. Rev. B **73**, 214209 (2006).
[34] H.-K. Kim, W.-S. Jung, and B.-J. Lee, Acta Mater. **57**, 3140 (2009).
[35] K.-H. Kang, I. Sa, J.-C. Lee, E. Fleury, and B.-J. Lee, Scr. Mater. **61**, 801 (2009).
[36] E. C. Do, Y.-H. Shin, and B.-J. Lee, J. Phys.: Condens. Matter **21**, 325801 (2009).
[37] H.-K. Kim, W.-S. Jung, and B.-J. Lee, J. Mater. Res. **25**, 1288 (2010).
[38] K. Chenoweth, A. C. T. van Duin, and W. A. Goddard, J. Phys. Chem. A **112**, 1040 (2008).
[39] J. E. Angelo, N. R. Moody, and M. I. Baskes, Modell. Simul. Mater. Sci. Eng. **3**, 289 (1995); M. I. Baskes, X. Sha, J. E. Angelo, and N. R. Moody, Modell. Simul. Mater. Sci. Eng. **5**, 651 (1997).
[40] Y. Q. Cheng, E. Ma, and H. W. Sheng, Phys. Rev. Lett. **102**, 245501 (2009).
[41] G. Bonny, R. C. Pasianot, N. Castin, and L. Malerba, Philos. Mag. **89**, 3531 (2009).
[42] B. Jelinek, "ASE Atomistic Potential Tests," `http://code.google.com/p/ase-atomistic-potential-tests` (2011).
[43] P. E. Blöchl, Phys. Rev. B **50**, 17953 (1994); G. Kresse and D. Joubert, Phys. Rev. B **59**, 1758 (1999).
[44] G. Kresse and J. Hafner, Phys. Rev. B **47**, 558 (1993); G. Kresse and J. Furthmüller, Phys. Rev. B **54**, 11169 (1996).
[45] J. P. Perdew, J. A. Chevary, S. H. Vosko, K. A. Jackson, M. R. Pederson, D. J. Singh, and C. Fiolhais, Phys. Rev. B **46**, 6671 (1992).
[46] H. J. Monkhorst and J. D. Pack, Phys. Rev. B **13**, 5188 (1976).
[47] B. Jelinek, J. Houze, S. Kim, M. F. Horstemeyer, M. I. Baskes, and S.-G. Kim, Phys. Rev. B **75**, 054106 (2007).
[48] T. Lee, M. I. Baskes, S. M. Valone, and J. D. Doll, "Atomistic modeling of thermodynamic equilibrium and polymorphism of iron," (2011), Los Alamos Preprint: LA-UR 11-03286.
[49] X.-Y. Liu, P. Ohotnicky, J. Adams, C. Rohrer, and R. Hyland, Surf. Sci. **373**, 357 (1997).
[50] A. F. Wright, Phys. Rev. B **74**, 165116 (2006).
[51] P. Tzanetakis, J. Hillairet, and G. Revel, Phys. Status Solidi B **75**, 433 (1976).
[52] K. M. Carling, G. Wahnström, T. R. Mattsson, N. Sandberg, and G. Grimvall, Phys. Rev. B **67**, 054101 (2003).
[53] T. Hehenkamp, J. Phys. Chem. Solids **55**, 907 (1994).
[54] D. A. Andersson and S. I. Simak, Phys. Rev. B **70**, 115108 (2004).
[55] S. Dannefaer, P. Mascher, and D. Kerr, Phys. Rev. Lett. **56**, 2195 (1986); J. Throwe, T. C. Leung, B. Nielsen, H. Huomo, and K. G. Lynn, Phys. Rev. B **40**, 12037 (1989).
[56] T. Hehenkamp, W. Berger, J.-E. Kluin, C. Lüdecke, and J. Wolff, Phys. Rev. B **45**, 1998 (1992).
[57] H. Krimmel and M. Fähnle, Phys. Rev. B **62**, 5489 (2000).
[58] M. I. Mendelev, D. J. Srolovitz, G. J. Ackland, D. Y. Sun, and M. Asta, Philos. Mag. **83**, 3977 (2003).
[59] G. J. Ackland, D. J. Bacon, A. F. Calder, and T. Harry, Philos. Mag. A **75**, 713 (1997).
[60] C. Domain and C. S. Becquart, Phys. Rev. B **65**, 024103 (2001).
[61] H.-E. Schaefer, K. Maire, M. Weller, D. Herlach, A. Seeger, and J. Diehl, Scr. Metall. **11**, 803 (1977).
[62] M. I. Mendelev, M. J. Kramer, C. A. Becker, and M. Asta, Philos. Mag. **88**, 1723 (2008).
[63] Y. Mishin, M. J. Mehl, D. A. Papaconstantopoulos, A. F. Voter, and J. D. Kress, Phys. Rev. B **63**, 224106 (2001).
[64] M. Timonova, B.-J. Lee, and B. J. Thijsse, Nucl. Instrum. Methods Phys. Res., Sect. B **255**, 195 (2007).
[65] S. Ryu, C. R. Weinberger, M. I. Baskes, and W. Cai, Modell. Simul. Mater. Sci. Eng. **17**, 075008 (2009).
[66] S. Ramos de Debiaggi, M. de Koning, and A. M. Monti, Phys. Rev. B **73**, 104103 (2006).
[67] G. P. Purja Pun and Y. Mishin, Acta Mater. **57**, 5531 (2009).
[68] N. Sandberg, B. Magyari-Köpe, and T. R. Mattsson, Phys. Rev. Lett. **89**, 065901 (2002).
[69] B. A. Gillespie, X. W. Zhou, D. A. Murdick, H. N. G. Wadley, R. Drautz, and D. G. Pettifor, Phys. Rev. B **75**, 155207 (2007).
[70] J. Tersoff, Phys. Rev. B **38**, 9902 (1988).
[71] P. Erhart and K. Albe, Phys. Rev. B **71**, 035211 (2005).
[72] O. K. Al-Mushadani and R. J. Needs, Phys. Rev. B **68**, 235205 (2003).
[73] S.-G. Kim, M. F. Horstemeyer, M. I. Baskes, M. Rais-Rohani, S. Kim, B. Jelinek, J. Houze, A. Moitra, and L. Liyanage, J. Eng. Mater. Technol. **131**, 041210 (2009).
[74] M. I. Mendelev, S. Han, D. J. Srolovitz, G. J. Ackland, D. Y. Sun, and M. Asta, Philos. Mag. **83**, 3977 (2003).
[75] S. L. Dudarev and P. M. Derlet, J. Phys.: Condens. Matter **17**, 7097 (2005).
[76] C.-C. Fu, F. Willaime, and P. Ordejón, Phys. Rev. Lett. **92**, 175503 (2004).
[77] B. J. Jesson, M. Foley, and P. A. Madden, Phys. Rev. B **55**, 4941 (1997).
[78] L. Vitos, A. V. Ruban, H. L. Skriver, and J. Kollár, Surf. Sci. **411**, 186 (1998).
[79] F. De Boer, R. Boom, W. Mattens, A. Miedema, and A. Niessen, *Cohesion in Metals: Transition Metal Alloys*, edited by F. R. de Boer and D. G. Pettifor, Vol. 1 (North-Holland, Amsterdam, 1988).
[80] J. H. Wilson, J. D. Todd, and A. P. Sutton, J. Phys.: Condens. Matter **2**, 10259 (1990).
[81] M. Timonova and B. J. Thijsse, Modell. Simul. Mater. Sci. Eng. **19**, 015003 (2011).
[82] A. A. Stekolnikov, J. Furthmüller, and F. Bechstedt, Phys. Rev. B **65**, 115318 (2002).
[83] D. J. Eaglesham, A. E. White, L. C. Feldman, N. Moriya, and D. C. Jacobson, Phys. Rev. Lett. **70**, 1643 (1993).
[84] X. Y. Liu, C. L. Liu, and L. J. Borucki, Acta Mater. **47**, 3227 (1999).
[85] P. Błoński and A. Kiejna, Surf. Sci. **601**, 123 (2007).
[86] H. Balamane, T. Halicioglu, and W. A. Tiller, Phys. Rev. B **46**, 2250 (1992).
[87] A. E. Mattsson and W. Kohn, J. Chem. Phys. **115**, 3441 (2001).
[88] R. Armiento and A. E. Mattsson, Phys. Rev. B **72**, 085108 (2005).
[89] J. P. Perdew, A. Ruzsinszky, G. I. Csonka, O. A. Vydrov, G. E. Scuseria, L. A. Constantin, X. Zhou, and K. Burke, Phys. Rev. Lett. **100**, 136406 (2008).
[90] A. E. Mattsson, R. Armiento, P. A. Schultz, and T. R. Mattsson, Phys. Rev. B **73**, 195123 (2006).

[91] R. Peierls, Proc. Phys. Soc. London **52**, 34 (1940).
[92] F. R. N. Nabarro, Proc. Phys. Soc. London **59**, 256 (1947).
[93] P. Carrez, D. Ferré, and P. Cordier, Modell. Simul. Mater. Sci. Eng. **17**, 035010 (2009).
[94] V. Vítek, Phys. Status Solidi **18**, 687 (1966).
[95] J. A. Zimmerman, H. Gao, and F. F. Abraham, Modell. Simul. Mater. Sci. Eng. **8**, 103 (2000).
[96] A. Datta, U. V. Waghmare, and U. Ramamurty, Acta Mater. **56**, 2531 (2008).
[97] M. Mihalkovic and M. Widom, "Alloy database," `http://euler.phys.cmu.edu/alloy/` (2009).
[98] C. Ravi, C. Wolverton, and V. Ozoliņš, Europhys. Lett. **73**, 719 (2006).
[99] C. Wolverton and V. Ozoliņš, Phys. Rev. Lett. **86**, 5518 (2001).
[100] J. L. Murray, Int. Met. Rev. **30**, 211 (1985).
[101] C. Ravi and C. Wolverton, Metall. Mater. Trans. A **36**, 2013 (2005).
[102] R. Besson and J. Morillo, Phys. Rev. B **55**, 193 (1997).
[103] L. Shaojun, D. Suqing, and M. Benkun, Phys. Rev. B **58**, 9705 (1998).
[104] W.-q. Zhang, Q. Xie, X.-j. Ge, and N.-x. Chen, J. Appl. Phys. **82**, 578 (1997).
[105] S. Meschel and O. Kleppa, Metall. Mater. Trans. A **22**, 2162 (1991).
[106] S. J. Solares, *Multi-scale simulations of single-walled carbon nanotube atomic force microscopy and density functional theory characterization of functionalized and non-functionalized silicon surfaces*, Ph.D. thesis, California Institute of Technology (2006).
[107] E. G. Moroni, W. Wolf, J. Hafner, and R. Podloucky, Phys. Rev. B **59**, 12860 (1999).
[108] S. Zhou, Y. Wang, F. Shi, F. Sommer, L.-Q. Chen, Z.-K. Liu, and R. Napolitano, J. Phase Equilib. Diffus. **28**, 158 (2007).
[109] S. Narasimhan and J. W. Davenport, Phys. Rev. B **51**, 659 (1995).
[110] Y. Zhong, M. Yang, and Z.-K. Liu, Calphad **29**, 303 (2005).
[111] N. Wang, W.-Y. Yu, B.-Y. Tang, L.-M. Peng, and W.-J. Ding, J. Phys. D: Appl. Phys. **41**, 195408 (2008).
[112] Y.-M. Kim, N. J. Kim, and B.-J. Lee, Calphad **33**, 650 (2009).
[113] X.-Y. Liu, P. P. Ohotnicky, J. B. Adams, C. L. Rohrer, and R. W. Hyland, Surf. Sci. **373**, 357 (1997).
[114] J. Murray, J. Phase Equilib. **3**, 60 (1982).
[115] P. Villars and L. D. Calvert, *Pearson's handbook of crystallographic data for intermetallic phases* (American Society for Metals, Materials Park, OH, 1985).
[116] D. Singh, C. Suryanarayana, L. Mertus, and R.-H. Chen, Intermetallics **11**, 373 (2003).
[117] S. G. Fries and T. Jantzen, Thermochim. Acta **314**, 23 (1998).
[118] X.-Y. Liu, *The development of empirical potentials from first-principles and application to Al alloys*, Ph.D. thesis, University of Illinois at Urbana-Champaign (1997).
[119] P. Maugis, J. Lacaze, R. Besson, and J. Morillo, Metall. Mater. Trans. A **37**, 3397 (2006).
[120] P. G. Gonzales-Ormeño, H. M. Petrilli, and C. G. Schön, Calphad **26**, 573 (2002).
[121] R. E. Watson and M. Weinert, Phys. Rev. B **58**, 5981 (1998).
[122] N. I. Kulikov, A. V. Postnikov, G. Borstel, and J. Braun, Phys. Rev. B **59**, 6824 (1999).
[123] M. Friák and J. Neugebauer, Intermetallics **18**, 1316 (2010).
[124] F. Lechermann, M. Fähnle, and J. M. Sanchez, Intermetallics **13**, 1096 (2005).
[125] C. L. Fu and M. H. Yoo, Acta Metall. Mater. **40**, 703 (1992).
[126] E. Lee and B.-J. Lee, J. Phys.: Condens. Matter **22**, 175702 (2010).
[127] X. SHU, W. HU, H. XIAO, H. DENG, and B. ZHANG, J. Mater. Sci. Technol. (Shenyang, China) **17**, 601 (2001).
[128] C. Vailhé and D. Farkas, Acta Mater. **45**, 4463 (1997).
[129] O. Kubaschewski and W. A. Dench, Acta Metall. **3**, 339 (1955).
[130] P. D. Desai, J. Phys. Chem. Ref. Data **16**, 109 (1987).
[131] R. Hultgren, P. D. Desai, D. T. Hawkins, M. Gleiser, and K. K. Kelley, *Selected values of the thermodynamic properties of binary alloys* (American Society for Metals, Metals Park, OH, 1973).
[132] W. Gale, C. Smithells, and T. Totemeier, *Smithells metals reference book* (Butterworth-Heinemann, 2004).
[133] W. B. Pearson, *A Handbook of lattice Spacings and Structures of Metals and Alloys* (Pergamon Press, New York, 1958).
[134] M. H. Yoo, T. Takasugi, S. Hanada, and O. Izumi, Mater. Trans., JIM **31**, 435 (1990).
[135] G. Simmons and H. Wang, *Single crystal elastic constants and calculated aggregate properties* (MIT Press, 1971).
[136] M. Krajčí and J. Hafner, J. Phys.: Condens. Matter **14**, 5755 (2002).
[137] N. P. Bailey, J. Schiøtz, and K. W. Jacobsen, Phys. Rev. B **69**, 144205 (2004).
[138] R. C. King and O. J. Kleppa, Acta Metall. **12**, 87 (1964).
[139] B. Predel and H. Ruge, Mater. Sci. Eng. **9**, 333 (1972).
[140] J. R. Davis, ed., *Metals Handbook Desk Edition*, 2nd ed. (ASM International, 1998).
[141] J. J. Chu and C. A. Steeves, J. Non-Cryst. Solids **357**, 3765 (2011).
[142] A. J. C. Wilson, Proc. Phys. Soc. **53**, 235 (1941).
[143] S. J. Plimpton, J. Comput. Phys. **117**, 1 (1995).
[144] S. R. Bahn and K. W. Jacobsen, Comput. Sci. Eng. **4**, 56 (2002).
[145] C. A. Becker, in *Models, Databases, and Simulation Tools Needed for the Realization of Integrated Computational Materials Engineering*, edited by S. M. Arnold and T. T. Wong (ASM International, 2011) Atomistic simulations for engineering: Potentials and challenges, `http://www.ctcms.nist.gov/potentials`.
[146] J. H. Rose, J. R. Smith, F. Guinea, and J. Ferrante, Phys. Rev. B **29**, 2963 (1984).
[147] F. D. Murnaghan, Proc. Natl. Acad. Sci. U. S. A. **30**, 244 (1944).